

FLUORESCENCE AND PHOTOGENERATION https://doi.org/10.1070/QEL16340

Study of the optical absorption and photoluminescence in $(Pb,Gd)_3(Al,Ga)_5O_{12}$:Ce epitaxial films grown from Pb-containing melt solutions

D.A. Vasil'ev, D.A. Spassky, S.I. Omelkov, N.V. Vasil'eva, A.V. Khakhalin, V.G. Plotnichenko

Abstract. **The optical absorption and photoluminescence properties of cerium-activated $(Pb,Gd)_3(Al,Ga)_5O_{12}$ epitaxial films are studied. The films are grown on single-crystal (111)-oriented $Gd_3Ga_5O_{12}$ substrates by liquid-phase epitaxy from supercooled $PbO-B_2O_3$ melt solutions at different concentrations of gadolinium, cerium, and aluminium oxides in the charge. The photoluminescence band of Ce^{3+} ions is shown to peak at 532 nm. The highest cathodoluminescence yield of about 51500 photons MeV^{-1} at a decay time of the slow component of 61.0 ns (light yield fraction 68 %) is found for the $Pb_{0.01}Ce_{0.03}Gd_{2.96}Al_{3.14}Ga_{1.86}O_{12}$ film, grown from melt solution with gadolinium oxide, cerium oxide, and aluminium oxide concentrations of 0.4, 0.2, and 4.5 mol % in the charge, respectively. Epitaxial films with these spectroscopic characteristics are promising for application in scintillation screens.**

Keywords: *optical absorption, luminescence, epitaxial films, garnet, cerium.*

1. Introduction

In view of the development of the technique for forming microimages by means of hard X-rays, it has become possible to use epitaxial films grown by liquid-phase epitaxy (LPE) in scintillation screens. These films should have a high light yield, low afterglow, high optical quality, high chemical stability and a thickness of no more than 20 μm; the emission spectrum should fall in the range of 400–700 nm to provide matching with a CCD camera. Lu_2SiO_5:Tb, $Lu_3Al_5O_{12}$:Eu, and $Gd_3Ga_5O_{12}$:Eu epitaxial films have been investigated as candidates for such screens [1]. The method of stimulated emission depletion (STED) was used to demonstrate the possibility of successful application of a Lu_2SiO_5:Tb epitaxial film and a STED laser, emitting at a wavelength λ = 628 nm [2]. The STED laser is used both to deplete stimulated emission and implement microscope resolution above the diffraction limit using selective photoluminescence quenching. Among garnet crystals, $Gd_3Al_2Ga_3O_{12}$: Ce (1 at %) (GAGG:Ce) single crystals are characterised by the highest light yield. To date, a 2-inch Czochralski-grown GAGG:Ce single crystal has demonstrated the highest light yield of about 58000 photons MeV^{-1} [3]. The scintillation luminescence decay time for the fast component in this crystal is 172 ns (light yield fraction η = 88 %) at λ = 516 nm. Introduction of divalent Ca or Mg ions into $Gd_3Al_2Ga_3O_{12}$:Ce (0.5 at %) single crystal leads to a decrease in the decay time [4]. Introduction of Mg causes a decrease in the decay time to 39.5 ns (η = 55 %) with a slight decrease in the light yield. Kamada et al. [4] attributed this decrease to the formation of Ce^{4+} centres, which trap electrons from the conduction band with subsequent fast light emission. The influence of Ce^{4+} centres on the luminescence intensity and the luminescence decay time was studied for garnet single crystals [5] and Y_2SiO_5:Ce and Lu_2SiO_5:Ce single-crystal films grown by LPE from PbO-containing melt [6].

GAGG:Ce garnet films, grown by LPE from the supercooled melt solution at gadolinium oxide, cerium oxide, and aluminium oxide concentrations of 0.2, 0.2, and 2.0 mol % in the charge, exhibited good scintillation properties [7]. Films grown from melt solution at gadolinium oxide, cerium oxide, and aluminium oxide concentrations of 0.4, 0.3, and 4.5 mol % found application as phosphors in the PIF-01 electron-optical converter [8]. It was shown in [9] that $Y_3Al_5O_{12}$ and $Lu_3Al_5O_{12}$ single-crystal garnet films, grown by LPE from $PbO-B_2O_3$ melt solution in platinum crucibles, have a number of unique advantages over bulk single crystals. These advantages are due to the absence of some structural defects that are characteristic of single crystals grown at higher temperatures. However, when epitaxial films are synthesised from $PbO-B_2O_3$ melt solutions, the films contain solvent components (as impurities): Pb^{2+} and Pb^{4+} ions [7] and Pt^{4+} ions, which arise as a result of dissolution of platinum crucible. The concentrations of these impurity ions can be controlled by changing the film growth temperature. For example, one can avoid incorporation of bound pairs of Pb^{2+} and Pb^{4+} ions into the film composition, in contrast to isolated Pb^{2+} ions [7, 10], which facilitate formation of Ce^{4+} centres.

Thus, we report the results of studying the optical absorption and photoluminescence in $(Pb,Gd)_3(Al,Ga)_5O_{12}$:Ce epitaxial films. The study was carried out to determine the composition of melt solution providing the highest photoluminescence intensity and light yield for the films grown.

D.A. Vasil'ev, N.V. Vasil'eva A.M. Prokhorov General Physics Institute, Russian Academy of Sciences, ul. Vavilova 38, 119991 Moscow, Russia; e-mail: dimaphys@gmail.com, natasha_v@lst.gpi.ru;
D.A. Spassky D.V. Skobeltsyn Institute of Nuclear Physics, M.V. Lomonosov Moscow State University, Vorob'evy gory, 119234 Moscow, Russia;
S.I. Omelkov Institute of Physics, University of Tartu, W. Ostwaldi str. 1, 50411, Tartu, Estonia; e-mail: omelkovs@gmail.com;
A.V. Khakhalin M.V. Lomonosov Moscow State University, Vorob'evy gory, 119991 Moscow, Russia; e-mail: avkhakhalin@mail.ru;
V.G. Plotnichenko Fiber Optics Research Center, Russian Academy of Sciences, ul. Vavilova 38, 119333 Moscow, Russia

Received 13 March 2017; revision received 6 June 2017
Kvantovaya Elektronika **47** (10) 922–926 (2017)
Translated by Yu.P. Sin'kov

2. Experimental

The $(Pb,Gd)_3(Al,Ga)_5O_{12}$:Ce films 10 × 15 mm in size were grown by the LPE method described in [7], from the supercooled $PbO-B_2O_3$ melt solution at concentrations $C(Gd_2O_3)$ = 0.2, 0.3, 0.4, and 0.5 mol %; $C(CeO_2)$ = 0.2 and 0.3 mol %; and $C(Al_2O_3)$ = 2.1, 4.0, and 4.5 mol % in the charge (Table 1). The substrates were 500-μm-thick single-crystal gadolinium–gallium garnet ($Gd_3Ga_5O_{12}$) substrates, oriented along the ⟨111⟩ direction. The film growth time was 5–210 min, and the substrate rotational speed was 50 or 132 rpm.

The total thickness $2h$ of the films grown on both substrate sides was determined by the weighing method. The thickness was calculated by neglecting the difference in the film and substrate densities. The chemical composition of the films was determined using a Quanta 3D FEG electron–ion scanning microscope (FEI, United States). Transmission spectra of the samples (film–substrate–film) were measured by a Lambda 900 spectrophotometer (PerkinElmer, United States) at 300 K in the wavelength range of 200–600 nm. The spectra of normalised optical density ($D/2h$) were calculated from the transmission spectra using the formula $D = \ln(T_{sub}/T_{sam})$, where T_{sub} and T_{sam} are, respectively, the substrate and sample transmittances as functions of the light wavelength. Photoluminescence spectra of the films were recorded at 300 K in the range of 400–700 nm upon excitation by a Heraeus D 200 VUV deuterium lamp at λ = 165 nm (7.5 eV), using a Hamamatsu H8259 photoelectron multiplier.

Photoluminescence excitation spectra were recorded at 300 K using the same lamp in the range of 260–500 nm; the excitation wavelength was λ = 540 nm (2.29 eV). The luminescence characteristics were measured using two monochromators: a primary monochromator McPherson Model 234/302 and a secondary monochromator Andor Shamrock 303i. The cathodoluminescence decay kinetics for cerium ions was measured with an interval of 5 nm in the range of 400–700 nm at 300 K on a pulsed cathodoluminescence system [11] equipped with a Radan-303A electron gun, characterised a polychromatic beam $80 < E_e < 120$ keV (de Broglie wavelength from 3.5 to 4.2 pm) and a single-pulse width of 300 ps. The measurements were performed using a Hamamatsu R3809U-50 photomultiplier and a LeCroy WavePro760Zi-A oscilloscope. The measured cathodoluminescence decay curves of the films were approximated by the sum of three exponentials: $I(t) = A_1\exp(-t/\tau_1) + A_2\exp(-t/\tau_2) + A_3\exp(-t/\tau_3)$ are the curve amplitudes and A_i are the decay time components (A_1, τ_2, and τ_3 are the slow, intermediate, and fast components, respectively; i = 1, 2, 3); the fraction of each component in the total emission yield was calculated from the formula $A_i\tau_i/(A_1\tau_1 + A_2\tau_2 + A_3\tau_3) \times 100\%$.

The values of the relative light yield for the grown films upon electron excitation were compared with the light yields of $Lu_{1.8}Y_{0.2}SiO_5$:Cee (LYSO:Ce) and CeF_3 single crystals, which were, respectively, ~27000 photons MeV^{-1} [12] and 4500 photons MeV^{-1} [13] upon excitation by 662-keV γ quanta. This method most likely gives somewhat overestimated light yield values, because it disregards the fact that the light yield does not change proportionally to the absorbed photon energy [14] with a change in the radiation energy and type; however, this method allows one to compare films reliably. To estimate the light yield, we chose films with a thickness larger than 40 μm, a value exceeding the electron beam penetration depth; in this case, the electron energy is completely absorbed in a film, as well as in a single crystal. At the same time, the light yield of the films excited by X-rays may be lower because of the larger X-ray penetration depth.

3. Results and discussion

We grew 33 samples of $(Pb,Gd)_3(Al,Ga)_5O_{12}$:Ce epitaxial films from melt solutions of six different compositions. For each composition, Table 1 contains experimental values of the maximum film thickness h_{max} and maximum growth rate f_g^{max}. Note that an increase in the concentration $C(Gd_2O_3)$ from 0.2 to 0.5 mol % in the melt solution leads to an increase in the saturation temperature by 134 °C and an increase in the film growth rate by 0.88 μm min^{-1}.

The normalised optical density spectra of the films with thicknesses $h < 15$ μm exhibit three absorption bands. The first band, peaking at 272.9 nm (4.5 eV), corresponds, according to [15], to the electronic transition of Pb^{2+} ($6s^2$) ions [Pb^{2+} ($6s^2$, $^1S_0$) → Pb^{2+} ($6s^1$ $6p^1$, $^3P_1$)]. The other two wide absorption bands in the ranges of 390–500 nm and 310–360 nm are due to interconfiguration electronic transitions 4f ($^2F_{5/2,7/2}$)–5d of Ce^{3+} ions (Fig. 1a).

The normalised optical density spectra of the films with thicknesses $h > 20$ μm, grown from compositions I, II, and VI, contain only two absorption bands of Ce^{3+} ions (Fig. 1b). An increase in the concentration ratio Al/Ga in a film from 0.74 [Fig. 1b, curve (*1*)] to 1.69 [curve (*2*)] leads to a red shift of the absorption band of the $5d_1$ level by 5.8 nm (see also Table 2). Note also a decrease in the intensity of the absorption band related to the $5d_2$ level in film VI-1 in comparison with the corresponding band in the spectra of films I-1 and II-1 [Fig. 1b, curve (*3*)].

Figure 1c shows the normalised optical density spectra of the films grown from compositions III–VI. The spectra contain the same absorption band due to Ce^{3+} ions; the absorp-

Table 1. Melt solution compositions and growth parameters of $(Pb,Gd)_3(Al,Ga)_5O_{12}$:Ce epitaxial films.

Melt solution No.	$C(Gd_2O_3)$ /mol %	$C(CeO_2)$ /mol %	$C(Al_2O_3)$ /mol %	δt/°C	Δt/°C	h_{max}/μm	f_g^{max}/μm min^{-1}
I	0.2	0.2	2.1	956–935	11–30	20.9	0.34
II	0.2	0.2	4.0	1013–1010	2–24	43.0	0.54
III	0.3	0.2	4.5	1057–1049	3–50	51.6	0.52
IV	0.4	0.2	4.5	1093–1065	17–76	90.8	1.44
V	0.4	0.3	4.5	1075–1065	5–25	67.7	0.80
VI	0.5	0.2	4.5	1083–1076	4–45	73.0	1.22

Note: δt is the temperature range containing the saturation temperature t_s; $\Delta t = t_s - t_g$ is the supercooling temperature (t_g is the growth temperature).

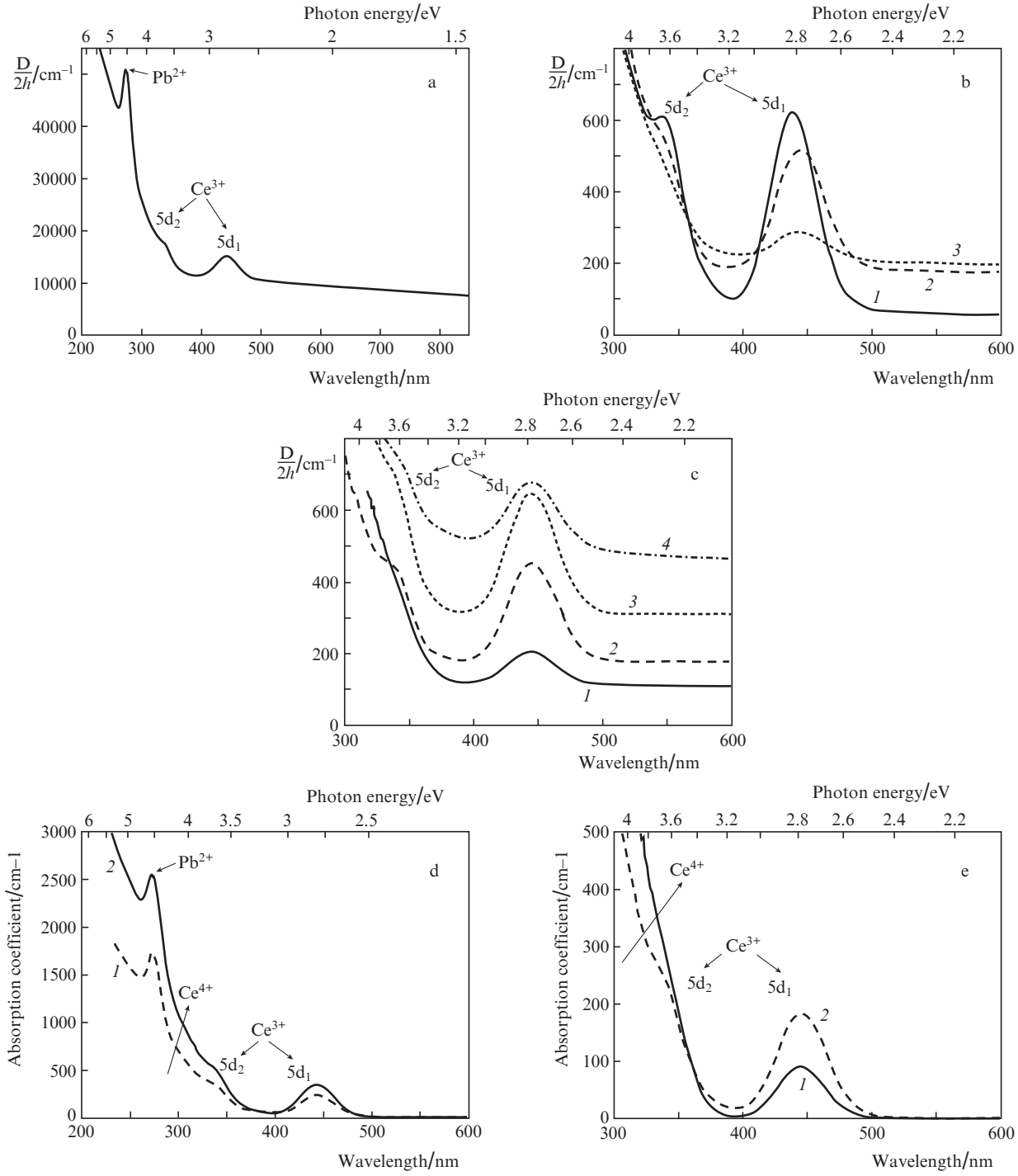

Figure 1. Spectra of normalised optical density D/2h of epitaxial films (a) II-2; (b) I-1 (*1*), II-1 (*2*), and VI-1 (*3*); and (c) VI-2 (*1*), V-1 (*2*), III-1 (*3*), and IV-2 (*4*) and absorption spectra of epitaxial films (d) IV-4 (*1*) and V-2 (*2*) and (e) VI-2 (*1*) and IV-2 (*2*) at $T = 300$ K (see Table 2).

tion band related to the $5d_2$ level is weaker for film VI-2 [Fig. 1c, curve (*1*)].

The absorption spectra of films IV-4 and V-2 are presented in Fig. 1d; they demonstrate enhanced absorption in the vicinity of 360 nm. The same increase in the region up to 360 nm (with a significant a decrease in the intensity of the absorption band of the $5d_2$ level) is observed in the absorption spectra of films IV-2 and VI-2 (Fig. 1e). The increase in absorption in this region with increasing concentration of doping divalent ions was observed in different matrices, for example, in $Gd_3Al_2Ga_3O_{12}$:Ce single crystals (1 at %) doped with Mg [16]; in $Lu_3Al_5O_{12}$:Ce optical ceramics doped with Mg [17]; and in polycrystalline $Lu_{0.8}Sc_{0.2}BO_3$:Ce (1 at %) powders doped with Ca, Mg, or Sr [18]. This phenomenon can be explained by the formation of Ce^{4+} centres and the occurrence of the related electron charge-transfer transition from the O^{2-} levels, located at the top of the valence band, to the levels of the Ce^{4+} ground state [17].

The photoluminescence and photoluminescence excitation spectra of the grown films are presented in Fig. 2. An excitation at $\lambda = 165$ nm (7.5 eV) gives rise to a wide photoluminescence band peaking near 532 nm (2.33 eV), which cor-

responds to the radiative transition $5d^1 \rightarrow 4f^1$ in Ce^{3+} ions. The intensity of this photoluminescence band was found to depend strongly on the melt solution composition and growth parameters. It was highest in the films grown from melt solution IV (see inset in Fig. 2 and Tables 1 and 2). The films grown from melt solutions V and VI were characterised by lower photoluminescence intensity. The photoluminescence excitation spectrum of film IV-2 in the wavelength range of 260–500 nm contains two bands peaking at 448 nm (2.77 eV) and 343 nm (3.61 eV), which are due to Ce^{3+} ions, and a wide band at 278 nm (4.46 eV), which are related to Pb^{2+} and Gd^{3+} ions (electronic transitions $^1S_0$ in Pb^{2+} ions and $^8S_{7/2}$ in Gd^{3+} ions [19]) [Fig. 2, curve (*3*)]. The presence of the latter band (at $\lambda = 278$ nm) is indicative of energy transfer from Gd^{3+} and/or Pb^{2+} ions to Ce^{3+}.

The positions of the maxima of the absorption band related to the $5d_1$ level and the photoluminescence band for film IV-2 were used to calculate the Stokes shift at 300 K. It turned out to be 0.46 eV for this film, a value much lower than that for $Gd_3Ga_2Al_3O_{12}$:Ce (1 at %) single crystal: 0.61 eV [20].

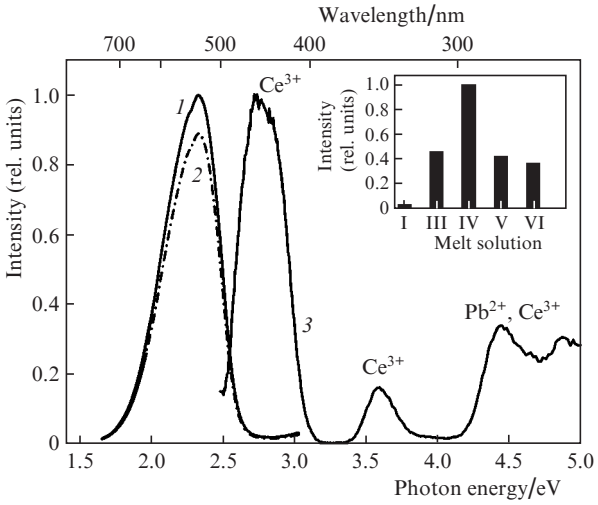

Figure 2. (*1*, *2*) Photoluminescence spectra of films (*1*) IV-1 and (*2*) IV-2 upon excitation at $\lambda = 165$ nm (7.5 eV) and $T = 300$ K and (*3*) photoluminescence excitation spectrum of epitaxial film IV-2 at $\lambda = 540$ nm (2.29 eV) and $T = 300$ K. The inset presents a comparison diagram of the maximum photoluminescence intensities for the $(Pb,Gd)_3(Al, Ga)_5O_{12}$:Ce films grown from melt solutions I, III, IV, V, and VI upon excitation at $\lambda = 344$ nm (3.6 eV) and $T = 300$ K.

Table 2 contains cathodoluminescence decay times with light yield fractions for each component. The decay times for epitaxial film IV-2, which exhibits the strongest luminescence, are $\tau_3 \sim 61$ ns, $\tau_2 \sim 24.9$ ns, and $\tau_1 \sim 2.1$ ns; the maximum light yield fraction (68 %) is observed for the slow component τ_3. Epitaxial films V-1 and VI-2 have the shortest decay times: $\tau_3 \sim 39$ ns, $\tau_2 \sim 11.1$ ns, and $\tau_1 \sim 1.7$ ns. The light yield is redistributed as follows: in films V-1 and VI-2, the maximum light yield fraction corresponds to the intermediate component τ_2 and amounts to 47 %, whereas in films III-1, IV-2, and IV-3 it corresponds to the component τ_3 and amounts to 60 %–70 %. Figure 3 shows the cathodoluminescence decay kinetics for films IV-2 and VI-2, which indicates a decrease in the decay time. The cathodoluminescence yields of the films, determined with respect to the LYSO:Ce single crystal, are listed in Table 2. It can be seen that the light yield is maximum (~51500 photons MeV^{-1}) for the $Pb_{0.01}Ce_{0.03}Gd_{2.96}Al_{3.14}Ga_{1.86}O_{12}$ film (IV-2). A comparison of the light yield of the same film with that of CeF_3 single crystal provided a somewhat smaller value (46000 photons MeV^{-1}), which allows one to estimate the instrumental error. The light yield for the films grown from melt solutions V and VI decreases almost by half. In addition, film IV-2 exhibits a decrease in the background level, which likely corresponds to the slower decay components (Fig. 3). This fact indicates that the presence of Ce^{4+} centres in the crystal also reduces the contribution of these slower decay components ($\tau > 200$ ns).

It follows from the measurements performed that the films grown from high-temperature melt solutions V and VI differ from the films grown from melt solution IV by the formation of Ce^{4+} centres, which cause a decrease in the photoluminescence intensity, relative light yield, and decay time and enhance absorption in the vicinity of 360 nm, which is accompanied by weakening of the absorption band related to the $5d_2$ level.

4. Conclusions

The study of the optical absorption and photoluminescence in the $(Pb, Gd)_3(Al, Ga)_5O_{12}$:Ce epitaxial films grown from Pb-containing melt solutions at concentrations $C(Gd_2O_3) =$

Table 2. Growth parameters of $(Pb,Gd)_3(Al,Ga)_5O_{12}$:Ce epitaxial films and their cathodoluminescence characteristics.

Sample No.	Film composition	h/μm	Δt/°C	λ_{Ce} ($5d_1$)/nm	$\tau_1\eta^{-1}$/ns %$^{-1}$	$\tau_2\eta^{-1}$/ns %$^{-1}$	$\tau_3\eta^{-1}$/ns %$^{-1}$	Light yield with respect to LYSO:Ce (in photons MeV^{-1})
I-1	$Pb_{0.04}Ce_{0.07}Gd_{2.89}Al_{2.13}Ga_{2.87}O_{12}$	20.9	21	438.7	–	–	–	–
II-1	$Pb_{0.01}Ce_{0.05}Gd_{2.94}Al_{3.14}Ga_{1.86}O_{12}$	43.0	4	444.5	–	–	–	–
II-2	$Pb_{0.06}Ce_{0.1}Gd_{2.84}Al_{3.14}Ga_{1.86}O_{12}$	5.2	2	444.5	–	–	–	–
III-1	$Pb_{0.01}Ce_{0.05}Gd_{2.94}Al_{3.14}Ga_{1.86}O_{12}$	51.6	47	444.5	2.5/3	22.3/42	57.1/55	~19500
IV-1	$Pb_{0.01}Ce_{0.02}Gd_{2.97}Al_{3.13}Ga_{1.87}O_{12}$	43.3	20	443.5	–	–	–	–
IV-2	$Pb_{0.01}Ce_{0.03}Gd_{2.96}Al_{3.14}Ga_{1.86}O_{12}$	40.7	31	444.5	2.1/2	24.9/30	61.0/68	~51500
IV-3	$Pb_{0.01}Ce_{0.06}Gd_{2.93}Al_{3.14}Ga_{1.86}O_{12}$	90.8	44	444.5	2.7/2	27.9/38	63.4/60	–
IV-4	$Pb_{0.01}Ce_{0.03}Gd_{2.96}Al_{3.14}Ga_{1.86}O_{12}$	14.3	22	444.5	–	–	–	–
V-1	$Pb_{0.01}Ce_{0.04}Gd_{2.95}Al_{3.14}Ga_{1.86}O_{12}$	67.7	25	444.5	1.7/11	11.1/47	38.7/42	~27000
V-2	$Pb_{0.01}Ce_{0.04}Gd_{2.95}Al_{3.13}Ga_{1.87}O_{12}$	5.0	5	443.5	–	–	–	–
VI-1	$Pb_{0.01}Ce_{0.03}Gd_{2.96}Al_{3.13}Ga_{1.87}O_{12}$	50.7	45	443.5	–	–	–	–
VI-2	$Pb_{0.01}Ce_{0.03}Gd_{2.96}Al_{3.12}Ga_{1.88}O_{12}$	73.0	28	443.3	1.7/11	11.2/47	39.1/42	~5700

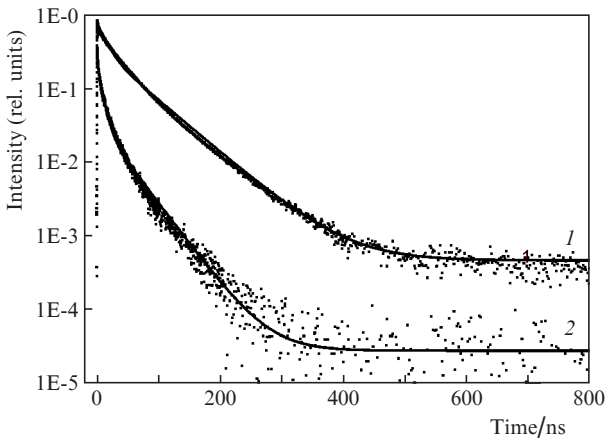

Figure 3. Cathodoluminescence decay kinetics for films (*1*) IV-2 and (*2*) VI-2 upon pulsed excitation by an electron gun with a single-pulse duration of 300 ps: (dots) experimental results and (solid line) approximation by the sum of three exponentials with decay times τ_1, τ_2, and τ_3. The slow-component decay time τ_3 is 61 and 39 ns for films IV-2 and VI-2, respectively.

0.2, 0.3, 0.4 and 0.5 mol %; $C(CeO_2)$ = 0.2 and 0.3 mol %; and $C(Al_2O_3)$ = 2.1, 4.0, and 4.5 mol % in the charge made it possible to determine the melt solution composition providing the strongest photoluminescence band of Ce^{3+} ions and the maximum cathodoluminescence yield (up to 51500 photons MeV^{-1}). These epitaxial films are promising for forming microimages using hard X-rays.

Acknowledgements. This work was supported by the European Social Fund's Doctoral Studies and Internationalisation Programme DoRa, Estonian Research Council (PUT1081), and (in part) Lomonosov Moscow State University Programme of Development.

References

1. Douissard P.-A., Cecilia A., Martin Th., Chevalier V., Couchaud M., Baumbach T., Dupre K., Kuehbacher M., Rack A. *J. Synchrotron Rad.*, **17**, 571 (2010).
2. Alekhin M.S., Patton G., Dujardin C., Douissard P.-A., Lebugle M., Novotny L., Stampanoni M.J. *Opt. Express*, **25**, 654 (2017).
3. Kamada K., Kurosawa Sh., Prusa P., Nikl M., Kochurikhin V.V., Endo T., Tsutumi K., Sato H., Yokota Yu., Sugiyama K., Yoshikawa A. *J. Opt. Mater.*, **36**, 1942 (2014).
4. Kamada K., Nikl M., Kurosawa Sh., Beitlerova A., Nagura Ay., Shoji Ya., Pejchal Ja., Ohashi Yu., Yokota Yu., Yoshikawa A. *J. Opt. Mater.*, **41**, 63 (2015).
5. Nikl M., Yoshikawa A. *Adv. Opt. Mater.*, **3**, 463 (2015).
6. Karner T., Laguta V.V., Nikl M., Shalapska T., Zazubovich S. *J. Phys. D: Appl. Phys.*, **47**, 065303 (2014).
7. Vasil'eva N.V., Spassky D.A., Randoshkin I.V., Aleksanyan E.M., Vielhauer S., Sokolov V.O., Plotnichenko V.G., Kolobanov V.N., Khakhalin A.V. *Mater. Res. Bull.*, **48**, 4687 (2013).
8. Vasil'ev D.A., Vereshchagin K.A., Vereshchagin A.K., Spassky D.A., Sokolov V.O., Khakhalin A.V., Vasil'eva N.V., Galstyan A.M., Plotnichenko V.G. *Prikl. Fiz.*, **4**, 5 (2015).
9. Zorenko Yu., Voloshinovskii A., Savchyn V., Voznyak T., Nikl M., Nejezchleb K., Mikhailin V., Kolobanov V., Spassky D. *J. Phys. Stat. Sol. (b)*, **244**, 2180 (2007).
10. Vasil'ev D.A., Spassky D.A., Voronov V.V., Sokolov V.O., Khakhalin A.V., Vasil'eva N.V., Plotnichenko V.G. *Neorg. Mater.*, **51** (10), 1090 (2015).
11. Omelkov S.I., Nagirnyi V., Vasil'ev A.N., Kirm M. *J. Luminesc.*, **176**, 309 (2016).
12. Moszynski M., Kapusta M., Mayhugh M., Wolski D., Flyckt S.O. *IEEE Transact. Nucl. Sci.*, **44**, 1052 (1997).
13. Auffray E., Baccaro S., Beckers T., Benhammou Y., Belsky A.N., Borgia B., Boutet D., Chipaux R., Dafinei I., de Notaristefani F., Depasse P., Dujardin C., El Mamouni H., Faure J.L., Fay J., Goyot M., Gupta S.K., Gurtu A., Hillemanns H., Ille B., Kirn T., Lebeau M., Lebrun P., Lecoq P., Mares J.A., Martin J.P., Mikhailin V.V., Moine B., Nelissen J., Nikl M., Pedrini C., Raghavan R. *Nucl. Instr. Meth. Phys. Res. A*, **383**, 367 (1996).
14. Khodyuk I.V., Dorenbos P. *IEEE Transact. Nucl. Sci.*, **59**, 3320 (2012).
15. Scott G.B., Page J.L. *J. Appl. Phys.*, **48**, 1342 (1977).
16. Kamada K., Shoji Y., Kochurikhin V.V., Nagura A., Okumura S., Yamamoto S., Yeom J.Y., Kurosawa S., Pejchal J., Yokota Y., Ohashi Y., Nikl M., Yoshino M., Yoshikawa A. *IEEE Transact. Nucl. Sci.*, **63** (2), 443 (2016).
17. Liu Sh., Feng X., Zhou Zh., Nikl M., Shi Yu., Pan Yu. *J. Phys. Stat. Sol. RRL*, **8** (1), 105 (2014).
18. Wu Yu., Ren G., Ding D., Zhang G., Shang Sh., Sun D., Pan Sh. *J. Opt. Mater.*, **35**, 520 (2013).
19. Randoshkin V.V., Vasil'eva N.V., Plotnichenko V.G., Pyrkov Yu.N., Lavrishchev S.V., Ivanov M.A., Kiryukhin A.A., Saletskii A.M., Sysoev N.N. *Fiz. Tverd. Tela*, **46**, 1001 (2004).
20. Ogiegło J.M., Katelnikovas A., Zych A., Justel Th., Meijerink A., Ronda C.R. *J. Phys. Chem. A*, **117**, 2479 (2013).